Arabian Journal of Chemistry (2020) **13**, 5199–5207

King Saud University

Arabian Journal of Chemistry

www.ksu.edu.sa
www.sciencedirect.com

ORIGINAL ARTICLE

Studies on molybdenum carbide supported HZSM-5 (Si/Al = 23, 30, 50 and 80) catalysts for aromatization of methane

Nagaraju Pasupulety *, Abdurrahim A. Al-Zahrani, Mohammad A. Daous, Hafedh Driss, Lachezar A. Petrov

Chemical and Materials Engineering Department, Faculty of Engineering, King Abdulaziz University, P.O. Box 80204, Jeddah 21589, Saudi Arabia

Received 13 January 2020; accepted 26 February 2020
Available online 6 March 2020

KEYWORDS

Molybdenum carbide;
Metallic molybdenum;
Methane;
Aromatization;
Benzene;
HZSM-5

Abstract Here in, for the first time we are reporting molybdenum carbide reduction into metallic molybdenum during methane aromatization on HZSM-5 (Si/Al ratio = 23, 30, 50 and 80) at methane space velocity of 1800 $mL.g_{cat}^{-}.h^{-}$. Benzene yield was influenced by the surface metallic molybdenum through the non-aromatic carbon deposits formation via linear hydrocarbons degradation on HZSM-5 with fewer acidity (Si/Al ratio = 30, 50 and 80). Our XPS analysis results demonstrated improved surface metallic molybdenum in spent Mo_2C/HZSM-5 = 80 (0.71 atom. %) and 50 (0.54 atom. %) samples over Mo_2C/HZSM-5 = 30 (0.33 atom. %) and 23 (0.20 atom. %) samples. Furthermore, HR-TEM and FFT analysis images clearly established fine distribution of distorted spherical shaped Mo_2C particles with 6–14 nm size in spent Mo_2C/HZSM-5 = 23. On the other hand, Mo_2C particle size was increased upto 22 nm in Mo_2C/HZSM-5 = 80. The ease reduction of Mo_2C into metallic molybdenum and aggregation of Mo_2C particles in spent higher Si to Al ratio (50 and 80) samples was associated with weak interactions between Mo_2C and the HZSM-5 with fewer acidity. At 700 °C, the order of benzene yield as follows: Mo_2C/HZSM-5 = 80 (2.2%) < Mo_2C/HZSM-5 = 50 (3.25%) < Mo_2C/HZSM-5 = 30 (5.2%) < Mo_2C/HZSM-5 = 23 (8.0%).

1. Introduction

Methane is the most abundant compound in natural gas has been considered as the world's third most important energy source followed by coal and oil (USGS Fact Sheet FS-113-01, 2002). Utilization of natural gas to value added products such as syngas, ethane, ethylene and aromatics (benzene, naphthalene etc.) has a significant impact on the world's

* Corresponding author.
E-mail address: nsampathra@kau.edu.sa (N. Pasupulety).
Peer review under responsibility of King Saud University.

Production and hosting by Elsevier

https://doi.org/10.1016/j.arabjc.2020.02.016
1878-5352 © 2020 Published by Elsevier B.V. on behalf of King Saud University.

energy balance (BP Statistical Review, 2013). However, the thermodynamic stability of methane is a challenging aspect to transform it into chemicals. Overall, the chemical activation of C—H bond (435 kJ/mol) in methane is an energy intensive process. Among the methane activation processes, direct methane conversion is economically attractive due to reduction in the oxygenated products. Presence of oxygen in the reaction steam drives the equilibrium to negative free energy. However, large amounts of CO_2 and H_2O formation limits its usage. Hence, non-oxidation of methane to aromatics attracted wide attention (Han et al., 1992).

Wang et al. (1993) was first reported non-oxidative methane dehydro-aromatization (MDA) using Mo/HZSM-5 catalyst in a continuous flow process. After this study, many reports were available in the literature using transition metal loaded zeolite catalyst systems for MDA process (Guo et al., 2014; Chu et al., 2010; Rodrigues et al., 2008; Wong et al., 2012; Cao et al., 2013). The main investigation aspects of these studies as follows: identification of suitable catalyst system, optimization of process, identification of molybdenum location and its interaction with zeolite, finding the active species, finding the reaction mechanism and the enhancement of catalyst performance. Here are some observations in non-oxidative MDA on transition metal loaded zeolite catalysts: (i) Mo/HZSM-5 acts as a bi-functional catalyst (ii) there is an induction period during which molybdenum oxide species is reduced by CH_4 to molybdenum carbide or molybdenum oxycarbide (iii) carbon deposits during the reaction process, which influences the catalytic activity and (iv) Mo interacts with alumina through dealumination process which also influences the performance of catalyst.

Various metal ions deposited on different supports have been investigated for non-oxidative MDA process which includes Mo, Zn (Liu et al., 2011; Luzgin et al., 2008), W (Kusmiyati et al., 2005; Kozlov et al., 2008), Re (Shu et al., 2003) and Cu, Mn, Ni, V and Ga (Tan et al., 2006). For instance, Xu et al. (1994) have studied the performance of Mo, Zn, Cu, Pt, and Ni metal ions deposited on HZSM-5 for MDA process. Weckhuysen et al. (1998) compared the performance of Mo, Fe, V, Cr and W deposited HZSM-5 catalysts in MDA reaction. Among the studied catalysts Mo/HZSM-5 was yielded good results at 750 °C with methane space velocity of 800 $mL.g^{-}.h^{-}$. Wang et al. (2000) reported that Re/HZSM-5 possess the similar catalytic performance as Mo/HZSM-5 at 750 °C. However its usage was limited by its availability. Further, different types of zeolites were studied in non-oxidative MDA process by Ma et al. (2013) and the resulted catalytic activity order as follows: HZSM-5 > HZSM-8 > HZSM-11 > HMCM-22 > MCM-41 > MCM-36 > MCM-49. Recently, Rahman et al. (2018) and Tan et al. (2019) respectively reported the catalytic activity of MoC_x/HZSM-5 = 30 and MoC_x/HZSM-5 = 25 catalysts for methane aromatization at 700 °C with methane space velocity of 1550 $mL.g_{cat}^{-}.h^{-}$. The authors attributed the catalytic activity to Mo_2C dispersion on HZSM-5. However, no chemisorption and or HR-TEM studies were performed to know the factual dispersion of Mo_2C. Tessonnier et al. (2008) pointed out the anchoring mode of molybdenum on HZSM-5 with different Si to Al ratio (15, 23 and 40). This study was lack interms of Mo_2C formation and its transformation during MDA on HZSM-5.

In the present study, we used different Si to Al ratio (23, 30, 50 and 80) HZSM-5 supports and 6 wt% of molybdenum was deposited on each of them by using wet impregnation method. The calcined catalysts were pre-carburized and subsequently methane aromatization activity was investigated at 700 and 750 °C with methane space velocity of 1800 $mL.g_{cat}^{-}.h^{-}$. A detailed characterization of support, calcined and spent catalysts were done by using BET-poresize, XRD, XPS, SEM-EDS, HR-TEM, EPR, NH_3-TPD-mass and TPO techniques. The role of metallic molybdenum due to the reduction of Mo_2C active phase and its resultant effect on carbon deposits formation was discussed further.

2. Experimental

HZSM-5 with different Si to Al ratio was obtained from Sigma-Aldrich and used without further purification. Sigma-Aldrich sample code CBV-2314 represents Si to Al ratio = 23; CBV-3024E represents Si to Al ratio = 30; CBV-5524G represents Si to Al ratio = 50 and CBV 8014 represents Si to Al ratio = 80. Ammonium heptamolybdate tetra hydrate $(NH_4)_6Mo_7O_{24}{\cdot}4H_2O$ (≥99.9%) precursor was also obtained from Sigma-Aldrich and used as a molybdenum source for Mo/HZSM-5 catalysts.

2.1. Catalyst synthesis

For nominal loadings of 6 wt% of molybdenum, about 1.104 g of ammonium heptamolybdate tetrahydrate was dissolved in 100 mL of deionized water. To this solution 9.4 g of HZSM-5 (Si/Al = 23, 30, 50 and 80) was added and the resultant mixture was aged for 2 h. The excess water was evaporated by using hot plate at 120 °C. The obtained solid particles were dried in a preheated oven at 110 °C. The dried samples were calcined at 500 °C in static air for 4 h. The resultant samples were denoted as MoO_3/HZSM-5 = 23 for 6 wt% of molybdenum deposited HZSM-5 with Si to Al ratio = 23 and so on so forth. Further, Mo/HZSM-5 catalyst denotation represents both MoO_3/HZSM-5 and spent Mo_2C/HZSM-5 samples respectively with Si to Al ratio = 23, 30, 50 and 80.

2.2. Carburization

For example, 0.5 g of calcined MoO_3/HZSM-5 = 23 was placed in a quartz reactor and CH_4/H_2 gas mixture in a volume ratio of 1/4 with a flow rate of 50 $mL.min^{-}$ was passed through the loaded sample. The reactor temperature was maintained at 700 or 750 °C for 30 min. Subsequently, the reactor was purged with N_2 gas at a flow rate of 20 mL min^{-} for 30 min followed by non-oxidative MDA reaction was carried out on these catalysts. Identical procedure was followed for the carburization of MoO_3/HZSM-5 catalysts with different Si to Al ratio.

2.3. Characterization of samples

All the studied HZSM-5 (with Si to Al ratio = 23, 30, 50 and 80), MoO_3/HZSM-5 and spent Mo_2C/HZSM-5 at 700 or 750 °C samples were characterized by using the following techniques.

The BET surface area-pore size analysis was done by using Quantachrome Nova Station (USA). The samples were

pretreated under vacuum for 2 h at 200 °C. XRD analysis was done by using EQUINOX 1000 Inel XRD machine at Co Kα = 1.7902 Å with acquisition of 2θ from 10° to 110°. XPS analysis was done by using SPECS GmbH analysis system containing Mg Kα 1253.6 eV X-ray source. The samples binding energy (BE) was attained by using C1s 284.8 eV correction.

NH_3-TPD and TPO analysis results were obtained by using micromeritics AutoChem HP 2950 V3.02 instrument. The mass spectral data was obtained by using ThermoStarTM GSD 320 quad core mass spectrometer. The m/z values followed were: m/z = 17 (NH_3), m/z = 18 (H_2O), m/z = 28 (CO) and m/z = 44(CO_2). In a typical experiment, spent samples of 100 mg each was placed in a quartz tube and pretreated at 200 °C in He flow (10 cm^3 min^{-1}) for 2 h. Subsequently, the temperature of the sample was brought to 40 °C and saturated with 5% NH_3-N_2 for 1 h. Then, the sample was purged with He flow (10 cm^3 min^{-1}) for 1 h. Desorption of ammonia was performed over the temperature range of 40–800 °C at a ramping rate of 10 °C min^{-1}. Desorption stream was analyzed simultaneously using a TCD and mass detector by means of an automated split valve.

For TPO experiments about 100 mg of each spent catalyst was loaded in quartz tube and 1%O_2-He gas mixture was used as a probe gas. Desorption of CO_2 was recorded over the temperature range of 40–800 °C at a ramping rate of 10 °C min^{-1}. Desorption stream was analyzed by TCD and mass detector.

SEM-EDX was done by using field emission scanning electron microscopy (FE-SEM, Quanta FEG450, FEI) equipped with an Everhart Thornley detector (ETD, HV mode) and a solid-state back scattering electron detector (VCD). High resolution transmission electron microscopy (HR-TEM) and fast fourier transform (FFT) results of spent Mo_2C/HZSM-5 = 23 and 80 was collected on Tecnai 200 kV D1234 SuperTwin microscope with camera length of 97 cm. EPR spectra were recorded by using JEOL JES-FA 100 EPR spectrometer operating in the X-band with standard TE_{011} cylindrical resonator at 123 K. TG/DTG analysis was carried out on STA-449 F3, NETZSCH instrument by using 20 mg of spent sample loading.

2.4. Activity tests

Catalytic activity tests were carried out in a continuous flow fixed bed quartz reactor at ambient pressure with methane GHSV of 1800 $mL.g_{cat}^{-}.h^{-}$. Pre-carburized catalyst at 700 or 750 °C was introduced with CH_4/N_2 gas mixture at a volume ratio of 9/1. The product stream was analyzed by a gas chromatograph equipped with a HaySep D 80/100 column, to analyze gases, such as H_2, N_2, CO, CO_2, CH_4, C_2H_4, and C_2H_6, by TCD and a HP-1 capillary column was used to analyze condensable aromatics, such as benzene, toluene, xylenes, naphthalene and methyl naphthalene by FID. The resultant catalysts were labeled as spent Mo_2C/HZSM-5 = 23, 700 °C, for 6 wt% of molybdenum deposited HZSM-5 with Si to Al ratio = 23 at 700 °C reaction temperature and spent Mo_2C/HZSM-5 = 23, 750 °C, for 6 wt% of molybdenum deposited HZSM-5 with Si to Al ratio = 23 at 750 °C reaction temperature and so on so forth.

$$\%\ \text{Conversion}\ CH_4 = \frac{\text{moles of}\ CH_{4\ \text{in}} - \text{moles of}\ CH_{4\ \text{out}}}{\text{moles of}\ CH_{4\ \text{in}}} \times 100$$

$$\%\ \text{Selectivity} = \frac{\text{moles of product}_{\ \text{out}}}{\text{moles of}\ CH_{4\ \text{in}} - \text{moles of}\ CH_{4\ \text{out}}} \times 100$$

$$\%\ \text{Yield} = \frac{\text{moles of product}_{\text{out}}}{\text{moles of}\ CH_{4\ \text{in}}} \times 100$$

3. Results and discussion

3.1. XRD studies

Powder X-ray diffraction analysis (XRD) results of HZSM-5 and Mo/HZSM-5 samples are presented in Fig. 1a–d. Essentially, support HZSM-5 demonstrated X-ray diffraction signals at 2θ = 9.8, 10.2, 28.0, 29.0 and 29.5° ascribed to

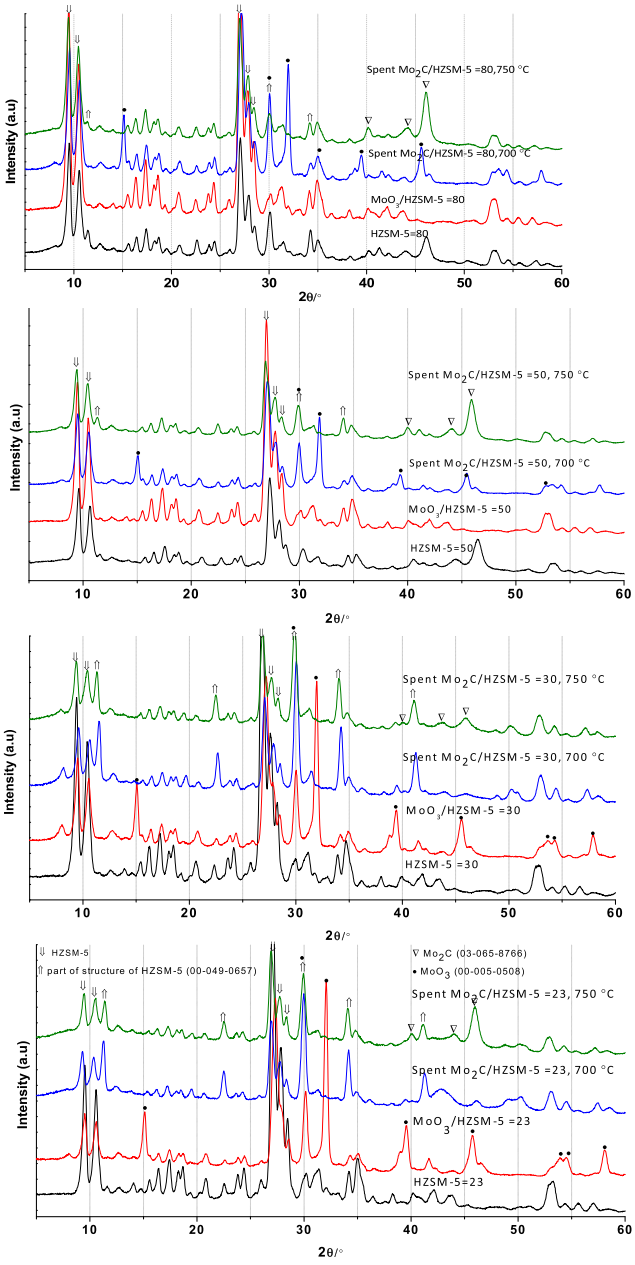

Fig. 1 XRD analysis of HZSM-5 and Mo/HZSM-5 samples.

zeolite framework (MFI). A part from zeolite signals, other X-ray signals related to MoO_3 (2θ = 30.5, 32.5, 39.8 and 46.0°) and Mo_2C (2θ = 40.0, 44.0 and 45.5°) phases were observed in Mo/HZSM-5 samples. Primarily, MoO_3 phase was observed in calcined MoO_3/HZSM-5 = 23 and 30 samples. Whereas, MoO_3 phase was not detected in MoO_3/HZSM-5 = 50 and 80 samples. It might be associated with the presence of small sized MoO_3 (< 4nm) crystals on high surface area HZSM-5 = 50 and 80. Evaluation of support, calcined and spent samples XRD results in Fig. 1a–d suggests Mo_2C phase formation was taken place by MoO_3 reduction under studied reaction conditions. However, presence of MoO_3 species in 700 °C spent Mo_2C/HZSM-5 = 50 and 80 samples emphasize partial reduction of MoO_3 into molybdenum carbide at this temperature. Further, at 750 °C, Mo_2C phase formation was facile over 700 °C spent Mo_2C/HZSM-5 samples. Interestingly, spent Mo_2C/HZSM-5 = 23 and 30 samples exhibited new X-ray diffraction signals at 2θ = 12.0, 22.0, 30.0, 34.0 and 42.5° are associated with part of HZSM-5 structure as reported in PDF-00-049-0657. On the other hand, X-ray diffraction signals related to part of HZSM-5 structure were minimized in spent Mo_2C/HZSM-5 = 50 and 80 samples. According to Gao et al. (2014) part of zeolite structure consists of external framework Al and Si sites which cut out from ZSM-5 zeolite cluster. Hence, in our case, part of HZSM-5 structure was observed after reaction suggests fraction of Mo species anchoring with extra-framework Al and Si sites in Mo_2C/HZSM-5 samples.

3.2. TEM/HR-TEM analysis

TEM and HR-TEM analysis of spent Mo_2C/HZSM-5 = 23 and 80 was presented as Fig. 2a–e. The TEM image in Fig. 2a shows finely distributed molybdenum carbide particles on the surface of HZSM-5. The distributed Mo_2C particles were sized in the range of 6–14 nm with distorted spherical shape. High resolution TEM image in Fig. 2b depicts the micro crystalline structure of molybdenum carbide with d spacing of ≈0.229 nm for crystalline plane (1 0 1) in Mo_2C. Further, FFT analysis (Fig. 2c and e) emphasizes Mo_2C (1 0 1) and HZSM-5 crystal plane existence in spent Mo_2C/HZSM-5 = 23 sample. Essentially, TEM analysis of spent Mo_2C/HZSM-5 = 80 (Fig. 2d) also showed fine distribution of Mo_2C particles with particle size between 6 and 22 nm. The increase in the Mo_2C particle size might be associated with its aggregation due to weak interactions with fewer acidity HZSM-5 = 80. It is obvious from these images that fine dispersion of Mo_2C particles on HZSM-5 in Mo_2C/HZSM-5 samples.

3.3. XPS analysis

XPS analysis of spent Mo_2C/HZSM-5 samples at 700 °C are presented as Fig. 3a–d. After deconvolution of XPS signal, Mo^{6+} (≈232.2 eV), Mo^{4+} (≈230.5 eV), Mo^{2+} (≈228.5 eV) and Mo^0 (≈227.2 eV) molybdenum species were observed in the studied samples. In general, existence of Mo^{6+} oxidation state for molybdenum suggests the presence of MoO_3. Whereas, Mo^{4+} oxidation state reflects the presence of MoO_2, a partially reduced species of MoO_3. Further, lower oxidation state molybdenum (Mo^{2+} and or Mo^{3+}) suggests the presence of Mo_2C in the studied samples (Oshikawa et al., 2001). Existence of Mo^0 suggests the metallic molybdenum species in the spent samples. However, surface metallic molybdenum formation was found high in higher Si to Al ratio samples over lower Si to Al ratio samples (Supplementary Table 1). It could be due to the ease reduction of Mo_2C species

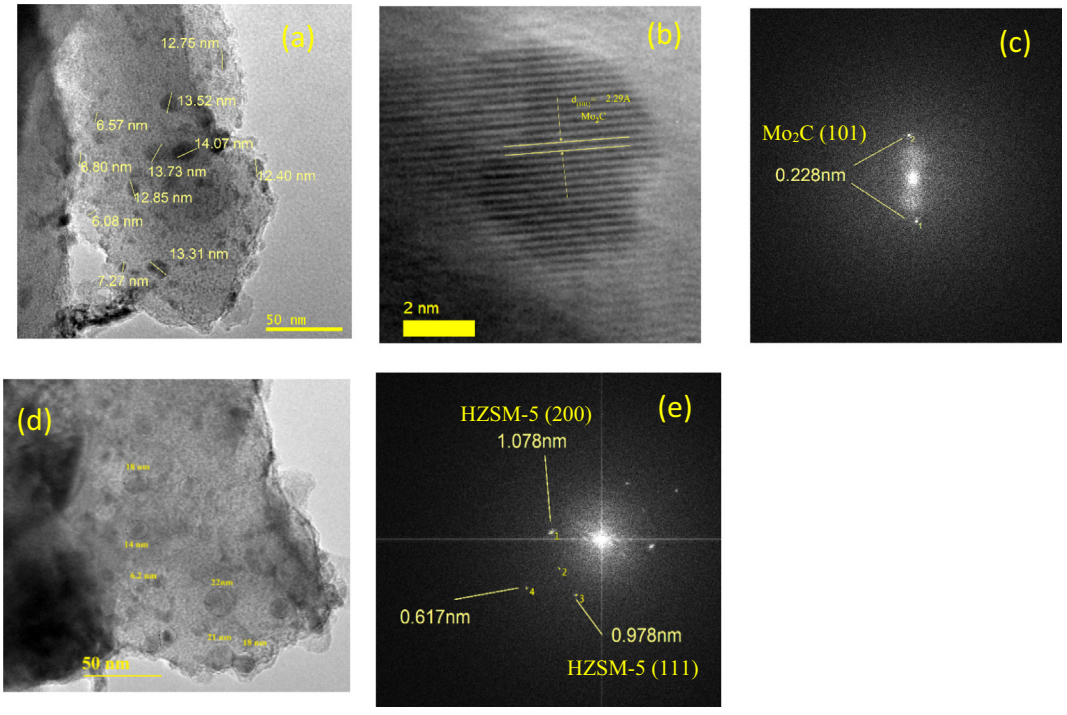

Fig. 2 (a) TEM analysis of Mo_2C/HZSM-5 = 23 (b) HR-TEM analysis of Mo_2C/HZSM-5 = 23 (c) FFT analysis for Mo_2C (d) TEM analysis of Mo_2C/HZSM-5 = 80 and (e) FFT analysis for HZSM-5.

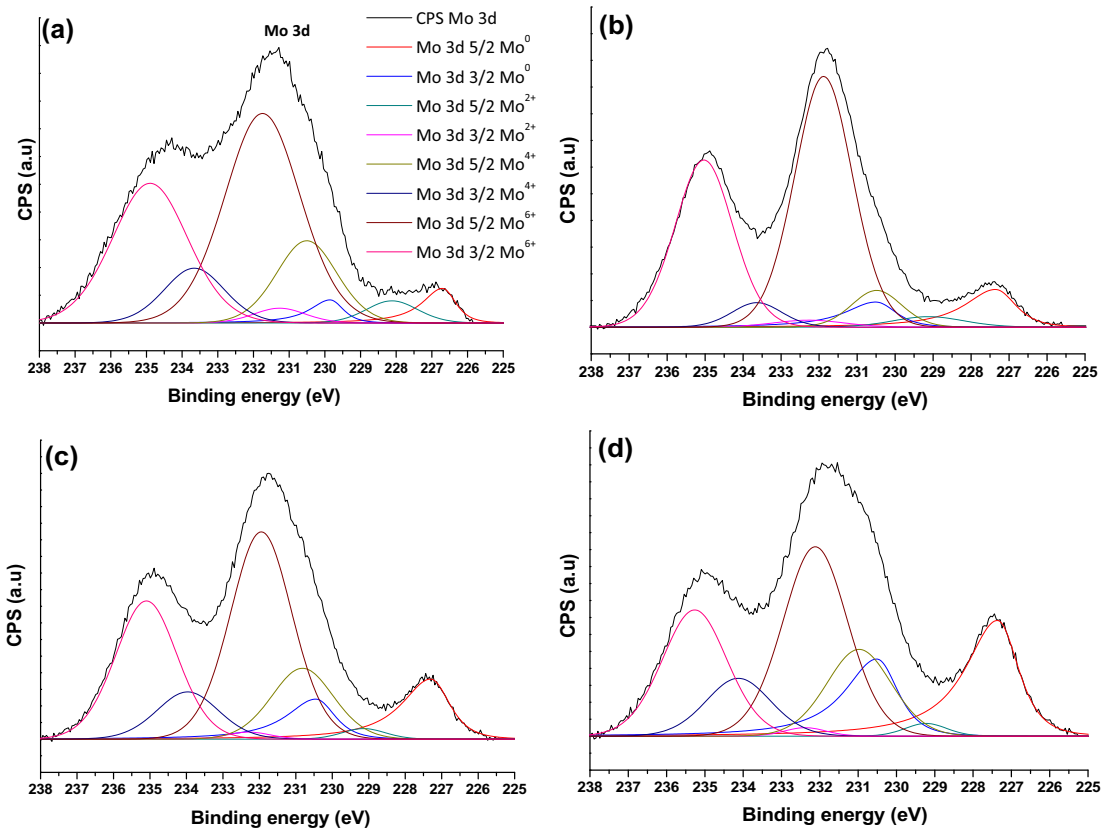

Fig. 3 XPS analysis of spent samples at 700 °C (a) Mo_2C/HZSM-5 = 23 (b) Mo_2C/HZSM-5 = 30 (c) Mo_2C/HZSM-5 = 50 and (d) Mo_2C/HZSM-5 = 80.

into metallic molybdenum for higher Si to Al ratio samples (Si/Al = 50 and 80) and associated with weak interactions between Mo_2C and HZSM-5 = 50 and 80 with fewer acidity. Moreover, slightly enhanced metallic molybdenum formation was observed in 750 °C spent Mo_2C/HZSM-5 = 50 and 80 samples suggests increase in the reaction temperature can also reduce Mo_2C into metallic Mo in these samples.

3.4. TPO studies

The nature of carbon deposits on spent Mo_2C/HZSM-5 samples were studied by TPO-mass technique (m/z = 44, CO_2) and the results are presented as Fig. 4. In general, carbon deposits formation in non-oxidative MDA was due to dehydrogenated methane ("CH_x") in parallel with desired C—C bond formation step on Mo_2C and or oligomerization of lower molecular weight intermediates ("C_2H_y") to desired product (benzene, naphthalene) on the Bronsted acid sites of zeolite (Spivey et al., 2014). Four types of CO_2 desorption signals were observed for spent Mo_2C/HZSM-5 = 23 and 30 samples respectively at T_{max} = 345, 440, 475 and 600 °C. On the other hand, only three types of CO_2 desorption signals were observed for Mo_2C/HZSM-5 = 50 & 80 samples at T_{max} = 340, 440 and 475 °C respectively. Among the CO_2 desorption signals, the maximum desorption was observed in the temperature range of 350–550 °C for all the studied samples. The CO_2, desorption upto 550 °C might be associated with more reactive coke that forms directly from dehydrogenated

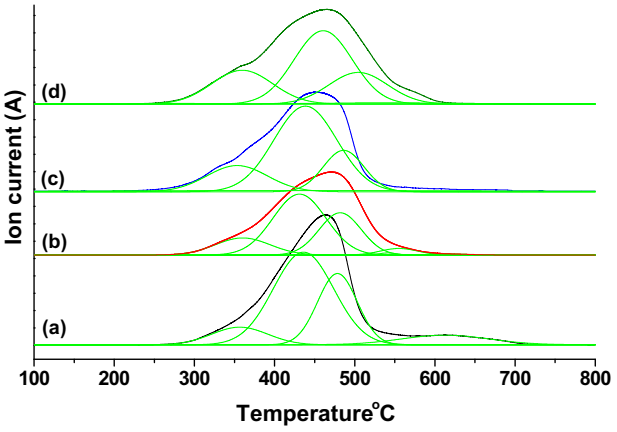

Fig. 4 TPO analysis of (a) Spent Mo_2C/HZSM5 = 23 (b) Spent Mo_2C/HZSM5 = 30 (c) Spent Mo_2C/HZSM5 = 50 (d) Spent Mo_2C/HZSM5 = 80 samples.

methane and or degradation of linear hydrocarbons on Mo_2C, metallic molybdenum and extra-framework Mo species. Desorption of CO_2 at about 600 °C might be associated with inert coke deposited on the Bronsted acid sites inside the zeolite channels (Tessonnier et al., 2008). Among the Studied catalysts the carbon deposits found high on spent Mo_2C/HZSM-5 = 80 (571 μmol g^{-1}) followed by Mo_2C/HZSM-5 = 50 (466 μmol g^{-1}), Mo_2C/HZSM-5 = 30

(428 μmol g^{-1}) and Mo_2C/HZSM-5 = 23 (390 μmol g^{-1}). It is obvious from the TPO results that non-aromatic carbon deposits (< 550 °C) formation was high in higher Si to Al ratio samples over lower Si to Al ratio ones.

3.5. NH_3-TPD-mass analysis

NH_3-TPD-mass analysis results are presented as Fig. 5. Two distinct ammonia desorption peaks were observed for all the spent Mo_2C/HZSM-5 samples. The first desorption was appeared in the temperature range of 75–275 °C with temperature maxima (T_{max}) about 140 °C. The second desorption was appeared in the temperature range of 325–575 °C with T_{max} about 350 °C. After deconvolution, six ammonia desorption peaks were observed for spent Mo_2C/HZSM-5 = 23 and 30 samples respectively at T_{max} about 135, 185, 270, 350, 390 and 490 °C. Whereas, five deconvolution signals were observed for spent Mo_2C/HZSM-5 = 50 and 80 samples at T_{max} about 120, 155, 230, 350 and 430 °C respectively. It is obvious from the results that ammonia desorption peaks were shifted to lower temperature with increase in the Si to Al ratio of HZSM-5. Acid sites of weak strength was reported in the temperature range of 150–190 °C and acid sites of strong strength was reported in the temperature range of 360–390 °C for HZSM-5 support through ammonia TPD analysis (Rodríguez-González et al., 2007). Acid sites of weak strength were attributed to silanol groups and the acid sites of strong strength were ascribed to bridging hydroxyl groups (Si-OH-Al) of HZSM-5 (Yu et al., 2019). On the other hand, calcined 4 wt% Mo/HZSM-5 = 15, 25 and 40 samples ammonia TPD analysis results yielded three desorption peaks at 200, 280 and 450 °C respectively for acid sites of weak, moderate (extra-framework aluminum) and very strong strength (located inside the channels of zeolite) (Tessonnier et al., 2008). Furthermore, bulk molybdenum carbide exhibited two distinct ammonia desorption peaks in the temperature range of 50–250 °C and 360–500 °C respectively (Bej et al., 2003). In the present study, the ammonia desorption below 150 °C might be associated with Mo_2C acid sites exhibited due to the charge transfer between molybdenum and C atoms (Bej et al., 2003). The remaining ammonia desorption peaks might be associated with HZSM-5 and or part of HZSM-5 structure with acid sites of weak, moderate, strong and very strong strength. The decreasing order of acidity for spent Mo_2C/HZSM-5 samples at 700 °C as follows: Mo_2C/HZSM-5 = 23 (856 μmol g^{-1}) > Mo_2C/HZSM-5 = 30 (646 μmol g^{-1}) > Mo_2C/HZSM-5 = 50 (393 μmol g^{-1}) > Mo_2C/HZSM-5 = 80 (277 μmol g^{-1}).

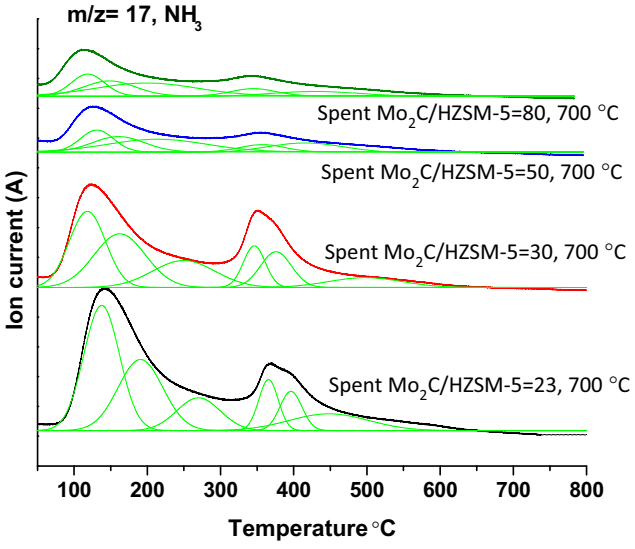

Fig. 5 NH_3-TPD-mass analysis of spent Mo_2C/HZSM-5 catalysts.

3.6. EPR studies

EPR spectra of spent Mo_2C/HZSM-5 samples are presented as Fig. 6. The EPR spectra was recorded in the magnetic field range of 300 to 360 mT. The intensive narrow EPR signal appeared at g factor equals to 2.00 was the characteristic band for carbon deposits in the studied samples. Apart from this signal, three more signals were observed for spent Mo_2C/HZSM-5 samples at g factor of 1.97, $g_{||}$ = 1.89 and $g_{\perp}$ = 1.93. EPR signal at 1.97 was observed for Mo/γ-Al_2O_3 system by Kostova et al. (2005) and it was attributed to the interaction between Mo and the support. Further, Kucherov et al. (2014) reported EPR signal at 1.96 for Mo/HZSM-30 system and attributed to the transition of molybdenum cations in the zeolite to paramagnetic Mo^{5+} ions under the reductive reaction atmosphere. Hence, in the present study, the signal observed at g factor of 1.97 is attributed to the presence of Mo^{5+} ions at the exchange sites of zeolite. On the other hand, the axial signal exhibited at $g_{||}$ = 1.8966 and $g_{\perp}$ = 1.9326 for Mo^{5+} paramagnetic ions was due to the aluminum molybdate ($Al_2(MoO_4)_3$) extra phase formed upon dealumination of the zeolite in the presence of molybdenum (Ha et al., 2013). However, all these signals were found weak in higher Si to Al ratio samples studied under identical EPR conditions. These results

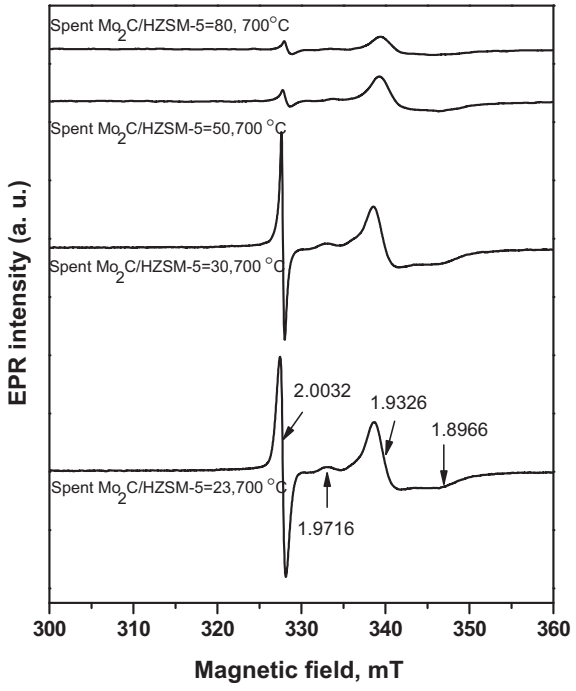

Fig. 6 EPR analysis of spent Mo_2C/HZSM-5 samples at 700 °C.

are in agreement with XRD data wherein, part of HZSM-5 structure was observed in spent Mo_2C/HZSM-5 samples.

4. Catalytic activity results

Catalytic activity results of Mo_2C/HZSM-5 catalysts are presented as Fig. 7a. Methane aromatization was performed at 700 and 750 °C with methane GHSV 1800 mL.g_{cat}^{-}.h^{-}. In general, Mo_2C/HZSM-5 catalytic activity in the dehydro-aromatization process was attributed to (i) active molybdenum carbide phase (ii) over all acidity of the catalyst. Fig. 7a shows the methane conversion at 700 and 750 °C over Mo_2C/HZSM-5 samples with different Si to Al ratio of HZSM-5. Greater methane conversions was observed at 750 over 700 °C under similar reaction conditions. Further, at both reaction temperatures, methane conversion was found high on lower Si to Al ratio Mo_2C/HZSM-5 catalysts over higher Si to Al ratio ones. The decreasing order of methane conversion at 750 °C for the studied catalysts as follows: Mo_2C/HZSM-5 = 23 (19%) > Mo_2C/HZSM-5 = 30 (16%) > Mo_2C/HZSM-5 = 50 (13.5%) > Mo_2C/HZSM-5 = 80 (11%). Similar conversion trend was observed for these catalysts studied at 700 °C. Liu et al. (1999) reported improved catalytic activity with respect to zeolite acidity in molybdenum impregnated HZSM-5 catalysts for methane aromatization. In 2008, Tessonnier et al. (2008) described that monomeric molybdenum anchoring on HZSM-5 played a major role in getting higher methane conversions. Further, Tan et al. (2019) stated that molybdenum dispersion was the significant factor for high conversion of methane in dehydro-aromatization process. Our HR-TEM analysis study (Fig. 2a–e) clearly demonstrated finely distributed molybdenum carbide particles with 6–14 nm size on the surface of HZSM-5 = 23 after 4 h of methane dehydro-aromatization process. Furthermore, NH_3-TPD-mass analysis results established greater acidity for lower Si to Al ratio samples over higher Si to Al ratio ones and showed greater catalytic activity.

Fig. 7b and c presents benzene, toluene, naphthalene and liner hydrocarbons selectivity (ethane and ethylene) on Mo_2C/HZSM-5 catalysts studied at 700 and 750 °C respectively. In general, methane aromatization takes place in two steps. In the first step methane dehydrogenation followed by C—C bond formation on Mo_2C led to ethylene formation. Then, in the second step, the ethylene is oligomerized into benzene on the Brønsted acid sites of the zeolite (Galadima et al., 2019). Greater benzene selectivity was observed on lower Si to

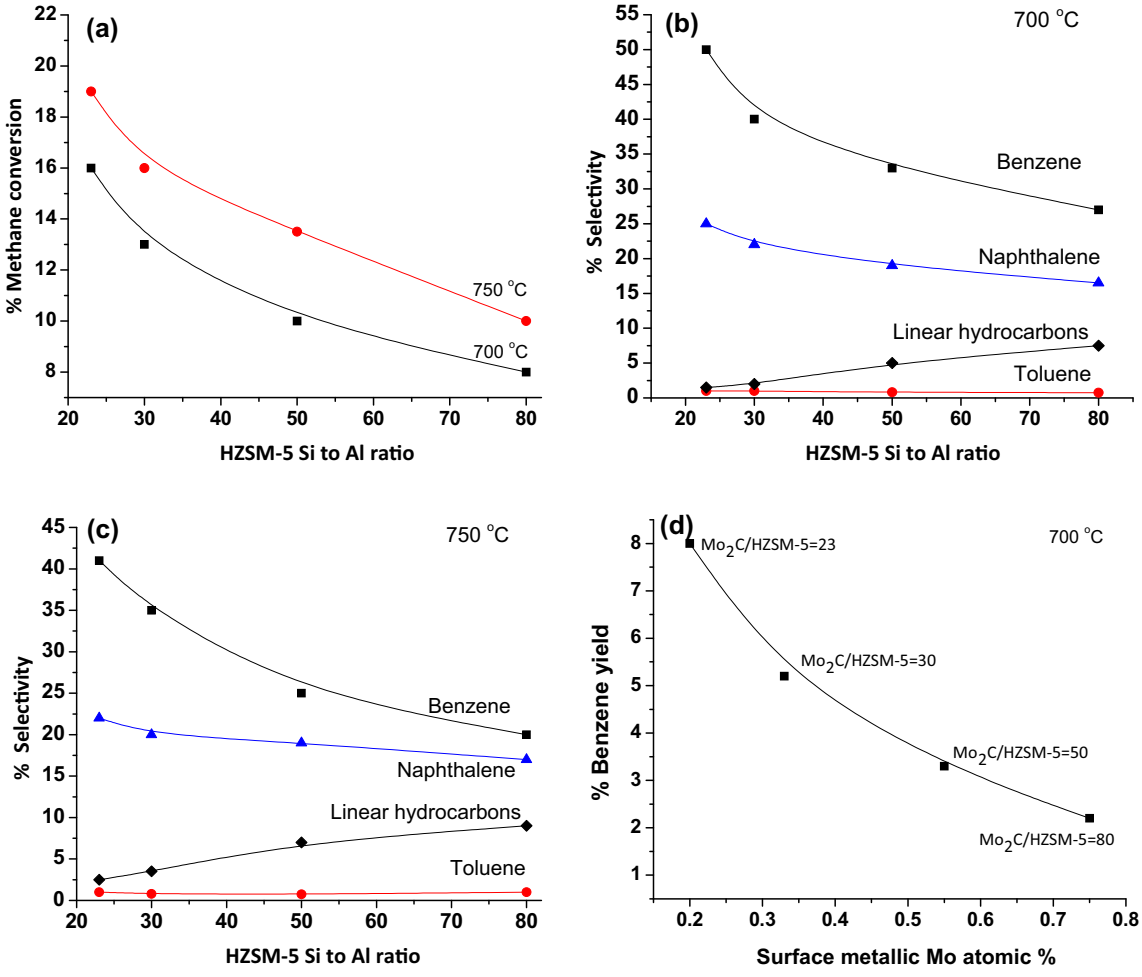

Fig. 7 (a) Aromatization activity of Mo_2C/HZSM-5 catalysts at methane GHSV 1800 mL.g_{cat}^{-}.h^{-} (b) Selectivity of aromatics and linear hydrocarbons on Mo_2C/HZSM-5 catalysts at 700 °C (c) Selectivity of aromatics and linear hydrocarbons on Mo_2C/HZSM-5 catalysts at 750 °C (d) Correlation between benzene yield and surface metallic molybdenum content of Mo_2C/HZSM-5 catalysts.

Al ratio Mo_2C/HZSM-5 catalysts compared to higher Si to Al ratio ones at both reaction temperatures. The decreasing order of benzene selectivity at 700 °C as follows: Mo_2C/HZSM-5 = 23 (50%) > Mo_2C/HZSM-5 = 30 (40%) > Mo_2C/HZSM-5 = 50 (33%) > Mo_2C/HZSM-5 = 80 (27%). Further, naphthalene selectivity was found high at lower Si to Al ratio catalysts compared to higher Si to Al ratio ones. The results suggest that benzene dimerization is favorable at lower Si to Al ratio Mo_2C/HZSM-5 catalysts. Essentially, toluene formation was about 1–1.5% in all the studied catalysts. Linear hydrocarbon formation was slightly improved for higher Si to Al ratio Mo_2C/HZSM-5 catalysts. It might be associated with high amount of surface metallic molybdenum found in these catalysts. It is well known that monometallic molybdenum-carbon catalysts improved the saturated hydrocarbon formation during CO hydrogenation process (Septilveda-Escribano et al., 1994). The enhancement of low temperature (350–550 °C) carbon deposits in higher Si to Al ratio Mo_2C/HZSM-5 catalysts through TPO analysis suggest that these carbon deposits were formed via dehydrogenated methane and or linear hydrocarbon degradation on Mo_2C and metallic molybdenum rather than from hydrogenated naphthalene during MDA. Solymosi et al. (1996) reported higher carbon deposits for Mo_2C/SiO_2 catalysts in the methane aromatization process. Hence, the selectivity of benzene was limited by metallic molybdenum in Mo_2C/HZSM-5 = 50 and 80 catalysts.

Methane dehydrogenation followed by C—C bond formation to ethylene on Mo_2C_x was reported as rate limiting step in non-oxidative MDA process (Tessonnier et al., 2008). In the present study the Mo_2C active phase was influenced by metallic molybdenum formation under the studied reaction conditions. Hence, the correlation was drawn between XPS surface metallic molybdenum content and benzene yield as Fig. 7d. Maximum benzene yield of 8% was observed on Mo_2C/HZSM-5 = 23 followed by Mo_2C/HZSM-5 = 30 (5.2%), Mo_2C/HZSM-5 = 50 (3.25%) and Mo_2C/HZSM-5 = 80 (2.2%). Decreased benzene yield on Mo_2C/HZSM-5 = 50 and 80 catalysts was associated with its greater metallic molybdenum content which catalyzes to carbon deposits through degradation of linear hydrocarbons. These results were in agreement with TPO data wherein, higher quantity of non-aromatic carbon deposits were observed for higher Si to Al ratio samples.

5. Conclusions

Mo_2C formation was facile at 750 °C on HZSM-5 = 50 and 80 supports respectively. Whereas, at 700 °C MoO_3 and Mo_2C phases were observed on these supports. Finely distributed Mo_2C particles with 6 to14 nm size was observed on Mo_2C/HZSM-5 = 23 spent catalyst and showed greater benzene yield of 8%. The decrease in the benzene yield was associated with greater amount of surface metallic molybdenum in Mo_2C/HZSM-5 = 50 and 80 catalysts. Ease reduction of Mo_2C to metallic molybdenum on Mo_2C/HZSM-5 = 50 and 80 catalysts essentially due to the weak interactions between Mo_2C and HZSM-5 = 50 and 80 supports with fewer acidity. The loss of methane aromatization activity was attributed to (i) surface metallic molybdenum (ii) aluminum molybdate formation.

Acknowledgements

This project was funded by the Deanship of Scientific Research (DSR) at King Abdulaziz University, Jeddah, under grant no. RG-08-135-38. The authors, therefore, acknowledge with thanks DSR for technical and financial support.

Appendix A. Supplementary material

Supplementary data to this article can be found online at https://doi.org/10.1016/j.arabjc.2020.02.016.

References

Bej, S.K., Bennett, C.A., Thompson, L.T., 2003. Acid and base characteristics of molybdenum carbide catalysts. Appl. Catal. A: Gen 250, 197–208. https://doi.org/10.1016/S0926-860X(02)00664-6.

BP Statistical Review of World Energy, 2013. Natural gas reserves. http://large.stanford.edu/courses/2013/ph240/lim1/docs/bpreview.pdf.

Cao, Z., Jiang, H., Luo, H., Baumann, S., Meulenberg, W.A., Caro, J., 2013. Natural gas to fuels and chemicals: improved methane aromatization in an oxygen-permeable membrane reactor. Angew. Chem. Int. Ed. 52, 13794–13797. https://doi.org/10.1002/anie.201307935.

Chu, N., Wang, J., Zhang, Y., Yang, J., Lu, J., Yin, D., 2010. Nestlike hollow hierarchical MCM-22 microspheres: synthesis and exceptional catalytic properties. Chem. Mater. 22, 2757–2763. https://doi.org/10.1021/cm903645p.

Galadima, A., Muraza, O., 2019. Advances in Catalyst design for the conversion of methane to aromatics: a critical review. Catal. Surv. Asia 23, 149–170. https://doi.org/10.1007/s10563-018-9262-5.

Gao, J., Zheng, Y., Fitzgerald, G.B., de Joannis, J., Tang, Y., Wachs, I.E., Podkolzin, G., 2014. Structure of Mo_2C_x and Mo_4C_x molybdenum carbide nanoparticles and their anchoring sites on ZSM-5 zeolites. J. Phys. Chem. C 118, 4670–4679. https://doi.org/10.1021/jp4106053.

Guo, X., Fang, G., Li, G., Ma, H., Fan, H., Yu, L., Ma, C., Wu, X., Deng, D., Wei, M., Tan, D., Si, R., Bao, X., 2014. Direct, nonoxidative conversion of methane to ethylene, aromatics, and hydrogen. Science 344, 616–619. https://doi.org/10.1126/science.1253150.

Ha, V.T.T., Sarioglan, A., Erdem-Senatalar, A., Taarit, Y.B., 2013. An EPR and NMR study on Mo/HZSM-5 catalysts for the aromatization of methane: investigation of the location of the pentavalent molybdenum. J. Mol. Catal. A: Chem. 378, 279–284. https://doi.org/10.1016/j.molcata.2013.06.020.

Han, S., Martenak, D.J., Palermo, R.E., Pearson, J.A., Walsh, D.E., 1992. The direct partial oxidation of methane to liquid hydrocarbons over HZSM-5 zeolite catalyst. J. Catal. 136, 578–583. https://doi.org/10.1016/0021-9517(92)90087-X.

Kostova, N.G., Spojakina, A.A., 2005. Effect of gamma irradiation on the properties of molybdenum containing catalysts. Optoelectron J. Adv. Mater. 7, 1347–1352. 10.1.1.535.7365.

Kozlov, V.V., Zaikovskii, V.I., Vosmerikov, A.V., Korobitsyna, L.L., Echevskii, G.V., 2008. Active sites of the methane dehydroaromatization catalyst W-ZSM-5: an HRTEM study. Kinet. Catal. 49, 110–114. https://doi.org/10.1134/S0023158408010138.

Kucherov, A.V., 2014. Effect of the formation of secondary pores in zeolite ZSM-5 on the properties of molybdenum-zeolite catalysts for methane aromatization. Russ. J. Phys. Chem. A 88, 386–392. https://doi.org/10.1134/S0036024414030170.

Kusmiyati, Amin, N.A.S., 2005. Dual effects of supported W catalysts for dehydroaromatization of methane in the absence of oxygen. Catal. Lett. 102, 69–78. https://doi.org/10.1007/s10562-005-5205-7.

Liu, S., Wang, L., Ohnishi, R., Ichikawa, M., 1999. Bifunctional catalysis of Mo/HZSM-5 in the dehydroaromatization of methane to benzene and naphthalene XAFS/TG/DTA/MASS/FTIR characterization and supporting effects. J. Catal. 181, 175–188. https://doi.org/10.1006/jcat.1998.2310.

Liu, B.S., Zhang, Y., Liu, J.F., Tian, M., Zhang, F.M., Au, C.T., Cheung, A.S.-C., 2011. Characteristic and mechanism of methane dehydroaromatization over Zn-based/HZSM-5 catalysts under conditions of atmospheric pressure and supersonic jet expansion. J. Phys. Chem. C 115, 16954–16962. https://doi.org/10.1021/jp2027065.

Luzgin, M.V., Rogov, V.A., Arzumanov, S.S., Toktarev, A.V., Stepanov, A.G., Parmon, V.N., 2008. Understanding methane aromatization on a Zn-modified high-silica zeolite. Angew. Chem. Int. Ed. 47, 4559–4562. https://doi.org/10.1002/anie.200800317.

Ma, S., Guo, X., Zhao, L., Scott, S., Bao, X., 2013. Recent progress in methane dehydroaromatization: from laboratory curiosities to promising technology. J. Ener. Chem. 22, 1–20. https://doi.org/10.1016/S2095-4956(13)60001-7.

Oshikawa, K., Nagai, M., Omi, S., 2001. Characterization of molybdenum carbides for methane reforming by TPR, XRD, and XPS. J. Phys. Chem. B 105, 9124–9131. https://doi.org/10.1021/jp0111867.

Rahman, M., Sridhar, A., Khatib, S.J., 2018. Impact of the presence of Mo carbide species prepared *ex situ* in Mo/HZSM-5 on the catalytic properties in methane aromatization. Appl. Catal. A: Gen. 558, 67–80. https://doi.org/10.1016/j.apcata.2018.03.023.

Rodrigues, A.C.C., Monteiro, J.L.F., 2008. The use of CH_4/H_2 cycles on dehydroaromatization of methane over MoMCM-22. Catal. Commun. 9, 1060–1065. https://doi.org/10.1016/j.catcom.2007.10.007.

Rodríguez-González, L., Marko, F.H., Rodríguez-Castellón, B.E., Jiménez-López, A., Simon, U., 2007. The acid properties of H-ZSM-5 as studied by NH_3-TPD and ^{27}Al-MAS-NMR spectroscopy. Appl. Catal. A: Gen 328, 174–182. https://doi.org/10.1016/j.apcata.2007.06.003.

Septilveda-Escribano, A., Rodriguez-Reinoso, F., 1994. Mo-promoted Fe/activated carbon catalysts for carbon monoxide hydrogenation. J. Mol. Catal. 90, 291–301. https://doi.org/10.1016/0304-5102(94)00015-8.

Shu, Y.R., Ohnishi, R., Ichikawa, M., 2003. Improved methane dehydrocondensation reaction on HMCM-22 and HZSM-5 supported rhenium and molybdenum catalysts. Appl. Catal. A: Gen. 252, 315–329. https://doi.org/10.1016/S0926-860X(03)00467-8.

Solymosi, F., Szoke, A., Cserenyi, J., 1996. Conversion of methane to benzene over Mo_2C and Mo_2C/ZSM-5 catalysts. Catal. Lett. 39, 157–161. https://doi.org/10.1007/BF00805576.

Spivey, J.J., Hutchings, G., 2014. Catalytic aromatization of methane. Chem. Soc. Rev. 43, 792–803. https://doi.org/10.1039/C3CS60259A.

Survey, USGS Fact Sheet FS-113-01, 2002. Natural gas production in the United States. p. 2. https://pubs.usgs.gov/fs/fs-0113-01/fs-0113-01.pdf.

Tan, P., 2019. Ammonia-basified 10 wt% Mo/HZSM-5 material with enhanced dispersion of Mo and performance for catalytic aromatization of methane. Appl. Catal. A: Gen 580, 111–120. https://doi.org/10.1016/j.apcata.2019.05.011.

Tan, P., Au, C.T., Lai, S.Y., 2006. Methane dehydrogenation and aromatization over 4 wt% Mn/HZSM-5 in the absence of an oxidant. Catal. Lett. 112, 239–245. https://doi.org/10.1007/s10562-006-0209-5.

Tessonnier, J.-P., Louis, B., Rigolet, S., Ledoux, M.J., Pham-Huu, C., 2008. Methane dehydro-aromatization on Mo/ZSM-5: about the hidden role of Brønsted acid sites. Appl. Catal. A: Gen. 336, 79–88. https://doi.org/10.1016/j.apcata.2007.08.026.

Wang, L., Tao, L., Xie, M., Xu, G., Huang, J., Xu, Y., 1993. Dehydrogenation and aromatization of methane under non-oxidizing conditions. Catal. Lett. 21, 35–41. https://doi.org/10.1007/BF00767368.

Wang, L., Ohnishi, R., Ichikawa, M., 2000. Selective dehydroaromatization of methane toward benzene on Re/HZSM-5 catalysts and effects of CO/CO_2 addition. J. Catal. 190, 276–283. https://doi.org/10.1006/jcat.1999.2748.

Weckhuysen, B.M., Wang, D., Rosynek, M.P., Lunsford, J.H., 1998. Conversion of methane to benzene over transition metal ion ZSM-5 zeolites: I. catalytic characterization. J. Catal. 175, 338–346. https://doi.org/10.1006/jcat.1998.2010.

Wong, K.S., Thybaut, J.W., Tangstad, E., Stöcker, M.W., Marin, G. B., 2012. Methane aromatisation based upon elementary steps: kinetic and catalyst descriptors. Micropor. Mesopor. Mater. 164, 302–312. https://doi.org/10.1016/j.micromeso.2012.07.002.

Xu, Y., Liu, S., Guo, X., Wang, L., Xie, M., 1994. Methane activation without using oxidants over Mo/HZSM-5 zeolite catalysts. Catal. Lett. 30, 135–149. https://doi.org/10.1007/BF00813680.

Yu, X., Liu, B., Zhang, Y., 2019. Effect of Si/Al ratio of high-silica HZSM-5 catalysts on the prins condensation of isobutylene and formaldehyde to isoprene. Heliyon 5, e01640. https://doi.org/10.1016/j.heliyon.2019.e01640.